Journal of Minerals and Materials Characterization and Engineering, 2019, 7, 385-403
https://www.scirp.org/journal/jmmce
ISSN Online: 2327-4085
ISSN Print: 2327-4077

Comparative Study of Thermal Comfort Induced from Masonry Made of Stabilized Compressed Earth Block vs Conventional Cementitious Material

Hassane Seini Moussa[1], Philbert Nshimiyimana[1,2*], Césaire Hema[1,3], Ousmane Zoungrana[1,4], Adamah Messan[1], Luc Courard[2]

[1]Institut International d'Ingénierie de l'Eau et de l'Environnement (2iE), Laboratoire Eco-Matériaux et Habitats Durables (LEMHaD), Rue de la Science, Ouagadougou, Burkina Faso
[2]Université de Liège (ULiège), Urban and Environmental Engineering (UEE), Liège, Belgium
[3]Université Catholique de Louvain (UCLouvain), Architecture et Climat, Louvain-La-Neuve, Belgium
[4]Université de Liège (ULiège), Service socio-anthropologie du développement, Liège, Belgium
Email: *pnshimiyimana@doct.uliege.be

How to cite this paper: Moussa, H.S., Nshimiyimana, P., Hema, C., Zoungrana, O., Messan, A. and Courard, L. (2019) Comparative Study of Thermal Comfort Induced from Masonry Made of Stabilized Compressed Earth Block vs Conventional Cementitious Material. *Journal of Minerals and Materials Characterization and Engineering*, **7**, 385-403.
https://doi.org/10.4236/jmmce.2019.76026

Received: August 3, 2019
Accepted: October 19, 2019
Published: October 22, 2019

Abstract

This paper investigates the stabilization effect on compressed earth blocks (CEB) produced from quartz-kaolinite rich earthen material stabilized with 0% - 25% calcium carbide residue (CCR). The paper evaluated various physico-thermal properties of the stabilized CEB and thermal comfort in the model building made of CEB masonry. The optical properties of CEB were evaluated from the mineral composition of the earthen material and CCR and apparent density of the CEB. A simulation was carried out on naturally ventilated model building whose masonry is made of CCR stabilized CEB comparing to the so-called conventional cementitious materials such as cement blocks and concrete. The results showed a decrease of the apparent density of the CEB from 2100 $kg \cdot m^{-3}$ for unstabilized CEB (0% CCR) to 1600 $kg \cdot m^{-3}$ for 25% CCR stabilized CEB. The thermal conductivity and depth of penetration of the heat flux on a 24 hours period of CEB respectively decreased from 1 $W \cdot m^{-1} \cdot K^{-1}$ and 12.7 cm for 0% CCR-CEB to 0.5 $W \cdot m^{-1} \cdot K^{-1}$ and 10.2 cm for 25% CCR-CEB. The emissivity, solar absorptivity and visible absorptivity of the CEB respectively decreased from 0.82, 0.82 and 0.82 for 0% CCR-CEB to 0.80, 0.64 and 0.64 for 25% CCR-CEB. The number of hours of warm and humid thermal discomfort was impacted for stabilized CEB based masonry in comparison with cement based masonry. The warm discomfort in building made of 20% CCR-CEB masonry was 400 hours lesser than that in building made of hollow cement blocks masonry. If air conditioning system is used to

keep the indoor temperature below 28˚C, the economy of 310,000 CFA francs (535 USD) is made every year on energy consumption for cooling in the model building made of 20% CCR-CEB masonry, corresponding to 9.6% less, with respect to that made of hollow cement blocks masonry.

Keywords

Calcium Carbide Residue, Compressed Earth Block, Cementitious Materials, Energy Plus Software, Thermal Comfort

1. Introduction

Rational management of energy in buildings is a major issue that should matter all development actors. To reach this aim, it is important to evaluate the energy performance of buildings so that their optimal designs could be carried out accordingly. In the perpetual quest for better efficiency, the optimal choice of construction materials plays a crucial role [1] [2]. Burkina Faso, like other Sahelian countries, faces the problems related to the use of ecological and thermal comfort inducing building materials relative to their accessibility on the local market. Indeed, the construction materials known to be ecological or comfortable such as renewable materials (timber, recycled timber) and insulation require expensive initial or maintenance cost.

Thus, cement based materials are the most used for wall constructions in urban areas, representing about 52% of building made with cement blocks comparing to only 28% of those made of earth blocks in Burkina Faso [3]. Among various earth blocks based building materials, compressed earth blocks (CEB) represent 56% [4]. Cement based materials have worse energy efficiency than earthen materials [5] [6] [7] [8]. In addition, the process of production of cement based materials is very polluting, without mentioning their relatively high cost [8]. The choice of CEB is guided by the fact that they are known to be more ecological than cement blocks or concrete [9] [10] [11] [12]. CEB are produced from raw earthen material that presents certain physical and geotechnical characteristics, mixed with water, and statically compressed at a pressure of about 10 bar. These CEB are very often stabilized with cement or lime as well as by-product materials to improve their physical, mechanical and durability characteristics, thus reaching the required standards [13].

In recent decades, some studies tried to evaluate the thermal comfort in building gained from constructing with cement or lime stabilized earth blocks [8]. Thermal comfort is defined by ASHRAE [14] by "that condition of mind which expresses satisfaction with the thermal environment and is assessed by subjective evaluation". Some industrial and agricultural by-products are known to be used as physico-mechanical stabilizers of CEB [15] [16] [17]. This is the case of coal-ash, plastic wastes, alkali-treated date palm fibers or cassava peels. Some studies using those products as stabilizers highlight their effect on the

thermo-physical and mechanical properties of the CEB. Instead of using industrial products (cement, lime) for stabilizing CEB, some researchers try to substitute them with agricultural and industrial by-product such as calcium carbide residue (CCR). Recently, the stabilization of CEB with lime rich-CCR in total substitution of pure industrial lime revealed its benefits for improving the compressive strength of CEB related to the pozzolanic reaction taking place mainly between clay and lime [18] [19]. Nevertheless, previous study did not evaluate the influence of CCR stabilization on the thermal performances of CEB.

The present study seeks to evaluate the influence of stabilization of CEB with CCR on their physical and thermal properties. It further assesses the thermal comfort induced in the model building made of CCR-stabilized CEB masonry in comparison with the so-called conventional materials (cement blocks, concrete and cement-stabilized CEB). The thermal comfort was assessed throughout simulations on model building using the software of EnergyPlus and diagram of GIVONI for evaluation of the thermal comfort.

2. Materials and Methods

2.1. Processing and Characterization of Raw Materials

The raw earthen material is a beige clayey soil extracted from the locality of Pabré (012˚31.397'N, 001˚34.373'W, and altitude of 297 m). Its lumps were crushed to release the elementary particles. It was dried and sieved to remove aggregates larger than 5 mm, in order to facilitate homogeneous mixing and interaction with the binder. The binder and stabilizer is calcium carbide residue (CCR), an industrial by-product. The CCR was collected from Burkina Industrial Gas (BIG) located in Kossodo (012˚25.935'N, 001˚29.374'W, alt. 301 m). It was milled and sieved to collect the passing on 125 μm. This CCR was previously found to contain more than 40% of calcium hydroxide [18]. Industrial cement, CEM IIA 42.5, commercially produced by CIMBURKINA was used as control stabilizer of CEB, as reference [6] [8]. Other reference properties of the different conventional materials have been taken from the literature.

The mineral composition was analyzed by the X-ray diffraction technique using the Brucker D8-Advance Eco 1.5 kW diffractometer equipped with a copper anode (Cu Kα λ = 1.54060 Å, 40 kV, 25 mA) and the Lynxeye xe detector in coupled $2\theta/\theta$ mode. Qualitative and semi-quantitative analysis of the spectra was performed using Diffrac.Eva V4.11 and Topas V5 software of Brucker based on the rietveld refinement method.

2.2. Production and Curing of CEB

Different formulas of CEB were elaborated by adding various mass percentages of CCR (0%, 5%, 10%, 15%, 20% and 25%) with respect to the dry mass of earthen material. CEB stabilized with 8% cement, which is commonly used for stabilization of CEB in the area of Ouagadougou, were produced as reference. Dry materials (earth + CCR/cement) were mixed until achieving homogeneous mix-

tures. Dry mixtures were mixed with appropriate amount of water, equivalent to the optimum water content (OWC of 16% - 20% for 0% - 25% CCR), required for achieving the maximum density for each formula. Specimens of CEB were produced by manual compression of the wet mixtures in 295 × 140 × 95 mm^3 mold and cured in polymeric bags to minimize the carbonation and loss of moisture necessary for the reaction to take place. The curing took place at ambient temperature in the laboratory (30˚C ± 5˚C) for 45 days for the specimens stabilized with the CCR and 28 days for those stabilized with cement, the period required to achieve more than 95% of the reaction [20].

2.3. Characterization of the Physico-Thermal Proprieties of CEB

Cured CEB were dried at 40˚C ± 2˚C until reaching constant mass. Apparent density of the dry CEB was determined through hydrostatic weighing and Equation (1) according to NF P18-459 [21]. Where, ρ_{app} is the apparent density of the dry sample (kg·m^{-3}); M_{dry} is the dry mass of the dry sample (g); ρ_{wat} is the density of water (kg·m^{-3}); $M_{sat.wat}$ is the mass of the saturated sample weighed in water (kg); $M_{sat.air}$ is the mass of the saturated sample weighed in air (kg).

$$\rho_{app} = \frac{M_{dry} \times \rho_{wat}}{M_{sat.air} - M_{sat.wat}} \quad (1)$$

Thermal effusivity, specific heat capacity, thermal conductivity, thermal diffusivity and depth of penetration of heat flux are the main thermal properties measured on the CEB. They are determined using the DEsProTherm (Dispositif d'Estimation des Propriétés Thermiques) system presented in **Figure 1**. The measurement of thermal effusivity (E, J·m^{-2}·K^{-1}·$s^{-1/2}$) was performed on single size samples (6 × 4 × 3 cm^3). The thickness of 3 cm does not allow the heat to cross through the sample. Moreover, the measurement of the heat capacity, equivalent of the specific heat (Cp, J·kg^{-1}·K^{-1}), was carried out on samples of size 6 × 4 × 1 cm^3 allowing the heat flux to cross through the sample [22]. Once these two parameters were obtained, the thermal conductivity (λ, W·m^{-1}·K^{-1}), thermal diffusivity (a, m^2·s^{-1}) and depth of penetration of the heat flux (δp, m) for the period of time T (s) of 24 hours were determined using Equations (2), (3) and (4), respectively.

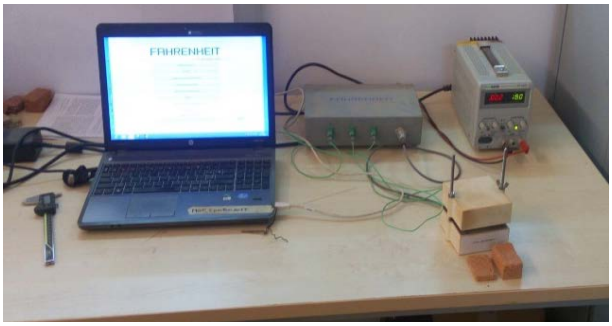

Figure 1. DesProTherm system for measurement of the thermal properties of CEB.

$$\lambda = \frac{E^2}{\rho_{app} \times C_p} \tag{2}$$

$$a = \frac{\lambda}{\rho_{app} \times C_p} \tag{3}$$

$$\delta_p = \sqrt{\frac{a \times T}{\pi}} \tag{4}$$

2.4. Estimation of the Optical Properties

The optical properties (emissivity, solar absorptance, visible absorptance) were estimated based on the mineral composition of the earthen material and CCR. Equation (5) presents the proportionality used to estimate the optical property (Op) of CEB with respect to the percent content (Ci) and optical property of the reference mineral (Opi) taken from the literature and libraries from Open studio and Energyplus [23]-[28]. The values obtained from this approximation were comparable with the values reported in the literature for the earthen materials [26] [28]. In addition, solar reflectance and visible transmittance values are assumed to be substantially the same [26] [29]. This approach was adopted given that the change in formula of CEB (different content of CCR) should logically have an impact on their optical properties. Thus, it would not be appropriate to consider the same value for all formulas of CEB. Other studies previously proposed alternative methods for determining the optical properties of material, but they require some specific equipment for measurement [30]. □

$$O_p = \sum \left(O_{p_i} \times C_i \right) \tag{5}$$

2.5. Description of the Model and Simulation Parameters

The building was modelled using SketchUP 2017 software. Once the model is elaborated, the properties of different construction elements, measured in the present study and collected from the literature, were defined. EnergyPlus software was used for thermal and energy simulation via the plug-in of Open Studio 2.8.0. XEsoView software was used to visualize the results of the simulation. The Givoni diagram was used for evaluation of the number of hours of thermal discomfort. This method was previously used for evaluation of the thermal comfort in the Sahelian and tropical contexts [23] [31] [32]. The Givoni diagram can be used to assess thermal comfort of occupants of a building by considering the data from the climate of the area, the activities of occupants inside the building and the expected indoor temperature and humidity [33] [34] [35].

The model building is a single-story building with four rooms, floor area of 185 m^2 and main facade toward the South. **Figure 2** and **Figure 3** respectively present the plan view and 3D view of the model building. The building has been modeled so that during simulations, only the characteristics of the masonry elements change from one variant of the model to another. The characteristics of the elements used in different variants of the model are summarized in **Table 1**.

The dimensions and positions of the bays are presented on the plane view (Figure 1). The windows are made with single glazing and outer doors are made of steel. The windows have a height of 1.2 m, placed at 1 m above the ground, except those in bathrooms that have a height of 0.7 m, placed at 1.5 m. All the doors have height of 2.2 m. Depending on the room and its use, the widths of windows and doors range between 0.6 m and 2 m such as shown in Figure 2. The model has a 1.5 mm thick corrugated steel sheet for the roofing and a 5 mm thick plywood ceiling placed 0.5 m below the roof. Table 2 presents the assumptions for the different schedules for the occupation and internal loads in the building. Note that these configurations are very common in the Sahelian region such as Burkina Faso. The parameters and assumptions made for modelling the building are summarized in Table 3.

Note that for the present simulations, the supply of cooling by devices such as air conditioners, humidifiers, is initially neglected for evaluating the thermal comfort induced by each masonry type. Only interactions between external conditions and materials are considered. The weather file used is that for Ouagadougou. The infiltration airflow rate is set at 0.5 $m^3 \cdot s^{-1}$ and mean velocity of the air is set at 0.3 $m \cdot s^{-1}$. The thermal resistance of the air gap (between the two steel sheets that constitute the external doors) is set at 0.16 $W \cdot m^{-1} \cdot K^{-1}$. The thermo-physical and optical properties of the conventional materials are given in Table 3.

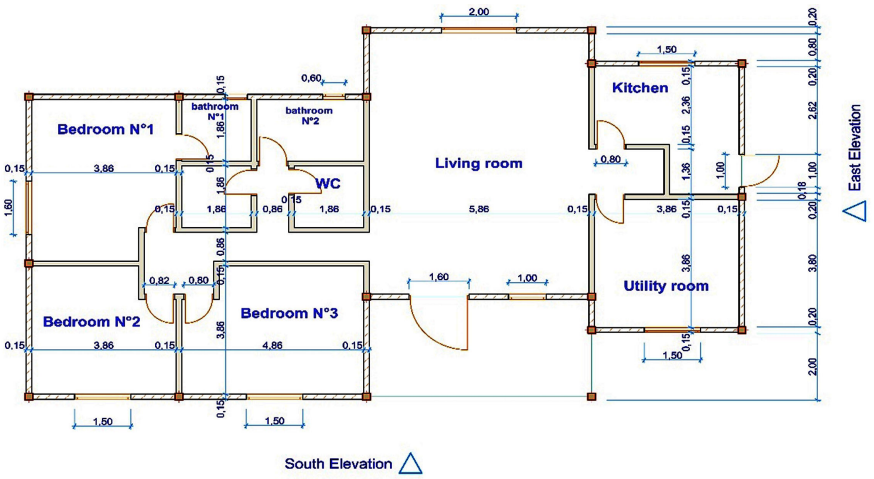

Figure 2. Plan view of the model building.

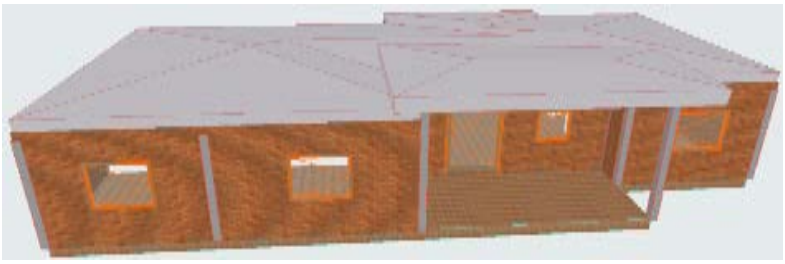

Figure 3. 3D view of the model building.

Table 1. Configurations of different variants of the model building.

Model	Description	Thick (cm)
M1	Basic model made of hollow cement blocks wall masonry of 40 × 20 × 15 cm^3 with 2 cm plaster (cement mortar) on both sides, a 1.5 mm steel sheet roof and a 5 mm plywood ceiling suspended 0.5 m below the roof. The external doors are made of steel in configuration of steel sheet-air-steel sheet and internal doors with steel frame and simple glazing.	19
M2	Same as M1, except that the masonry is made with plain cement blocks of 40 × 20 × 20 cm.	20
M3	Same as M1, except that the wall is made of reinforced concrete of 15 cm of thickness.	15
M4	Same as M1, except that the masonry is made with 8% CEM CEB.	20
M5	Same as M1, except that the masonry is made with 0% CCR CEB.	20
M6	Same as M1, except that the masonry is made with 5% CCR CEB.	20
M7	Same as M1, except that the masonry is made with 10% CCR CEB.	20
M8	Same as M1, except that the masonry is made with 15% CCR CEB.	20
M9	Same as M1, except that the masonry is made with 20% CCR CEB.	20
M10	Same as M1, except that the masonry is made with 25% CCR CEB.	20

Table 2. Planning of occupations and loads in the model building.

Planning	Schedule	Activity	Hypothesis
Occupant presence	00 h - 07 h	100%	Night and preparation
	07 h - 12 h	0%	External activities
	12 h - 14 h	100%	Lunch and nap
	14 h - 18 h	50%	Various activities (outdoor and indoor)
	18 h - 00 h	100%	Dinner and night
People activity (6 occupants)	00 h - 04 h	80 W/person	Sleeping
	04 h - 22 h	120 W/person	Normal activity
	22 h - 00 h	100 W/person	Moderated activity
Lighting (8 $W \cdot m^{-2}$)	04 h - 06 h	100%	Daybreak
	06 h - 18 h	0%	Sun shines
	18 h - 22 h	100%	Evening
	22 h - 04 h	0%	Night (sleeping)
Electrical appliances and boiler	Appliances such as refrigerators and heaters are supposed to be placed on the outside terraces. There is no boiler room.		
Air infiltration	It is assumed that air infiltrates the space 24/7.		
Temperature schedule	Indoor temperature was set at 28˚C, assumed as the temperature for air conditioning systems in most households in Ouagadougou (arbitrary benchmark for comparison of cost of energy consumption on cooling in different models)		

Table 3. Thermo-physical and optical properties of materials [23]-[28].

Properties of materials	Hollow block	Plain block	Concrete	OBS (plywood)	Plaster (mortar)	Concrete (floor)	Steel sheet
e (cm)	15	20	15	0.5	2	10	0.15
λ ($W \cdot m^{-1} \cdot K^{-1}$)	0.9	1.15	2.5	0.14	1.15	1.7	50
ρ ($kg \cdot m^{-3}$)	2100	2300	2400	600	1950	2300	7800
Cp ($J \cdot kg^{-1} \cdot K^{-1}$)	600	717	900	2300	846	850	115
α_{th}	0.85	0.87	0.93	0.7	0.85	0.9	0.7
α_s	0.64	0.66	0.7	0.75	0.64	0.65	0.9
α_v	0.64	0.66	0.7	0.75	0.64	0.65	0.9

The thickness of the glazing material, e is 0.3 cm, its thermal conductivity, λ is 0.93 $W \cdot m^{-1} \cdot K^{-1}$, its solar transmittance at normal incidence, g is 0.86, its visible transmittance at normal incidence, τl is 0.9. The front and back side infrared hemispherical emissivity, ε of the glazing material is 0.92, its front side solar reflectance at normal incidence FSSR index is 0.07 and its front side visible reflectance at normal incidence FSVR index is 0.08. The back side solar reflectance at normal incidence BSSR and back side visible reflectance at normal incidence BSVR indexes of this material are null. For the windows and frame of the door, the thickness is taken as 1.35 cm, its solar absorptivity and visible absorptivity indexes are set at 0.9. The front and back side infrared hemispherical emissivity value of the frame is 0.7. The width of the frame is 5 cm and its thermal transmittance Uf value is 3.3 $W \cdot m^{-2} \cdot K^{-1}$.

The thermal comfort assessment was based on the analysis computer program EnergyPlus 9.1.0 [29] and ASHRAE Standard 55 [14]. EnergyPlus evaluates the outdoor air temperature based on the input weather file, the indoor relative humidity and temperature depending on the activity of the occupants and internal thermal loads. Then the number of hours of discomfort are assessed based on the diagram proposed by Givoni [37]. This diagram presents boundaries of comfort zones, which are based on air temperature and air relative humidity (**Figure 4**). The black boundary limits the comfort zone for a null value of the velocity of the air. Every point that is inside that boundary represents an hour at which 90% of the occupants feel comfortable, according to the Predicted Mean Vote (PMV) [14]. The blue boundary limits the comfort zone for a velocity of air assumed at 0.3 $m \cdot s^{-1}$. Depending on the velocity of air, this zone may become thinner or larger.

From the diagram, out of the comfort zones, it can be inferred four zones of discomfort. Over the upper limit of the comfort zone is the humid discomfort zone. A point localized in that zone is considered non-comfortable hour because of high rate of humidity in the air. At the right side of the comfort zone is the warm (hot) discomfort zone. A point localized in that zone is considered non-comfortable because the temperature of the air is too high. Those situations, can cause health problems and harm the occupants body [38]. At the opposite,

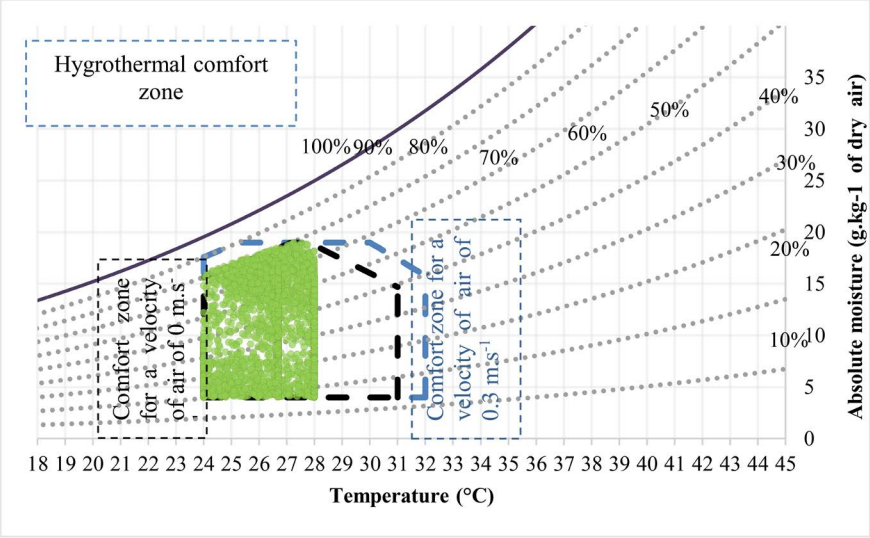

Figure 4. Givoni's bioclimatic diagram considering the air velocity of 0.3 $m \cdot s^{-1}$.

below the lower and left limit of the boundary of the comfort zone, are respectively located the dry and cold zone of discomfort. Those areas are also non-comfortable because of low rate of humidity in the air and low temperature of the air. The objective is to get most of the points that represents the hours of the year in the comfort zone considering a mean velocity of the air of 0.3 $m \cdot s^{-1}$. The other points should preferably be localized next to the comfort zone. The relative proximity of hours of discomfort to the comfort zone is assessed through the Hygrothermal Index (HI). This index, considering the combined effect of temperature and humidity, indicates whether a point is closer to the comfort zone or not. The lower the HI, the closer the points are to the comfort zone and the lesser aggressive is the discomfort.

2.6. Evaluation of the Cost of Energy Consumption

The evaluation of the cost was carried out on the energy that would be consumed when Air Conditioning System (ACS) is used to keep the indoor temperature not higher than 28˚C in each variant of the model building. This calculation is based on the output amount of energy needed to cool down the indoor environment assessed from EnergyPlus. The cost was estimated based on the value of the energy needed for cooling at efficiency of the ACS assumed at 83% and price of 96 CFA francs (0.17 USD) for 1 kWh of electricity [39].

3. Results and Discussions

3.1. Proprieties of the Materials

Table 4 presents the mineral composition of the earthen material and CCR. The earthen materials mainly contain quartz (63%) and kaolinite (30%) while the CCR mainly contains portlandite (43%), calcite and other carbonate minerals (50%). The optical properties such as the emissivity, solar absorption and visible

absorption of CEB, approximated through the proportionality method, are presented in Table 5. It shows that the addition of CCR improves the optical properties of the CEB. The solar transmittance, thermal absorptivity (emissivity of the material) and visible absorptivity of the CEB decreased respectively from 0.82, 0.82 and 0.82 for the non-stabilized (0%) CEB to 0.80, 0.64 and 0.64 for 25% CCR stabilized CEB (Table 5).

Table 5 furthermore shows that the CCR-stabilized CEB have lower apparent density than the non-stabilized CEB and cementitious materials. The apparent density varies between 1820 kg·m^{-3} and 1600 kg·m^{-3} for 5% - 25% CCR-stabilized CEB compared to more than 2100 kg·m^{-3} for non-stabilized CEB (0% CCR). This phenomenon can be partly explained by the fact that the specific density of CCR particles (2.49 g·cm^{-3}) is less than that of the earthen particles (2.66 g·cm^{-3}). Moreover, the decrease of the apparent density of CEB with CCR stabilization can be related to the increase of the OWC (16% - 20%) for production of CEB stabilized with 0% - 25% CCR. This resulted in increase of the total porosity of CEB from 30% to 40% for 5% - 25% CCR compared to 20% for 0% CCR stabilized CEB. The apparent density and thickness of the envelope materials are very relevant parameters for the thermal comfort of the building.

Table 4. Mineral composition of the raw materials.

Minerals	Earthen material	CCR
Quartz	63	3
K-Feldspar	7	-
Kaolinite	30	4
Portlandite	-	43
Aragonite	-	21
Calcite	-	16
Rapidcreekite	-	13
Total	100	100

Table 5. Physical, thermal and optical proprieties of CEB.

Properties of materials	8% CEM CEB	0% CCR CEB	5% CCR CEB	10% CCR CEB	15% CCR CEB	20% CCR CEB	25% CCR CEB
e (cm)	20	20	20	20	20	20	20
λ (W·m^{-1}·K^{-1})	0.78	1	0.69	0.66	0.6	0.47	0.52
ρ (kg·m^{-3})	1860	2117	1820	1741	1691	1629	1610
Cp (J·kg^{-1}·K^{-1})	846	808	812	876	905	938	848
αth	0.8	0.82	0.81	0.81	0.8	0.8	0.8
αs	0.75	0.82	0.78	0.74	0.71	0.67	0.64
αv	0.75	0.82	0.78	0.74	0.71	0.67	0.64

Additionally, the stabilization of CEB with CCR resulted in the decrease of the thermal conductivity from 1 $W \cdot m^{-1} \cdot K^{-1}$ for the 0% CCR-CEB to 0.5 $W \cdot m^{-1} \cdot K^{-1}$ for 25% CCR-CEB. These values are much lower than those for materials containing cement (2.5 $W \cdot m^{-1} \cdot K^{-1}$ for concrete). Furthermore, the heat capacity of CCR (0% - 25%) stabilized CEB ranged in 800 - 900 $J \cdot kg^{-1} \cdot K^{-1}$ compared to 900 $J \cdot kg^{-1} \cdot K^{-1}$ for concrete (Table 5). It is important to remind that the thermal properties "e, λ, ρ, and Cp" have been measured in the laboratory and the optical properties "αth, αs and αv" have been calculated through the method explain in paragraph II.4

3.2. Evaluation of the Thermal Discomfort

Figure 5 shows the evolution of the percentage of number of hours of thermal discomfort, warm, humid, other types, for the reference model (M1) and other variants. The total number of hours of thermal discomfort is about 64% for all models without air conditioning system. The predominant type of this discomfort is humid (wet), then warm and other types (dry and cold). In the area of Ouagadougou, it is the hot temperature of the air that worries more when referring to the thermal comfort of the buildings. The interest of representing the planning of occupation (Table 2) that reflects the habits of most people in the study area is to reflect the thermal discomfort that approaches the realities of the area. Compared to M1, out of all the 10 models, the model M9 (20% CCR-CEB masonry) has the lowest number of hours of warm discomfort.

While Figure 5 shows the cumulative number of discomfort hours, Figure 6 shows the relative number of hours of discomfort of different models with respect to the model M1. Negative values are favorable in a sense that they indicate that the percentage of hours of discomfort decreased. The thermal comfort can only be evaluated by the appreciation of the discomfort because it is a subjective sensation. The lower the relative discomfort induced from each model, the better the masonry behaves in term of the thermal performance comparative to the model M1. The model M9 (20% CCR CEB) has the lowest number of hours of warm discomfort. It records 21.2% lesser number of hours of warm discomfort compared to M1 (cement blocks), equivalent to a total of about 400 hours of warm discomfort in the year (Figure 5).

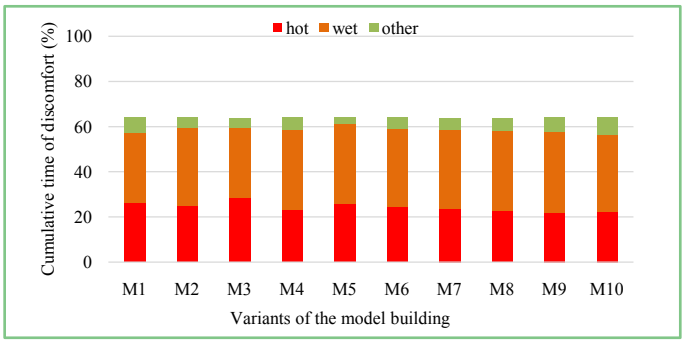

Figure 5. Percentage number of hours of thermal discomfort for different models.

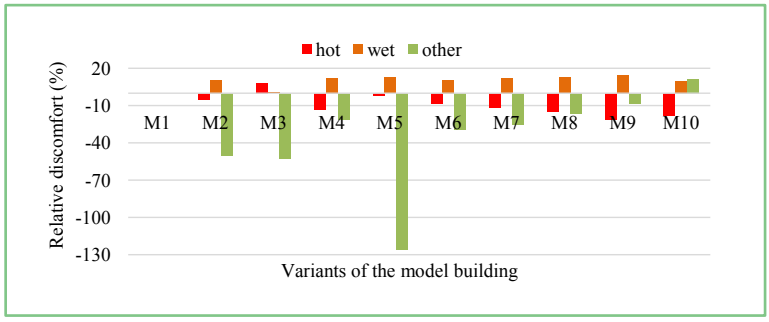

Figure 6. Relative number of hours of thermal discomfort for different models with respect to M1.

The number of hours of humid discomfort is relatively higher with CEB comparative with cement blocks (up to 14.6% higher for the model M9 vs model M1). The increasing humidity in the indoor environment can be explained by the relative high hygroscopic inertia of the masonry blocks. This was previously reported that the moisture content is closely related to the hygroscopic inertia of the building material in the studies which tried to show the relation between the hygroscopic inertia of the envelop and moisture content in a room [40] [41] [42].

To prevent or minimize the humid discomfort, natural and cost effective means exist such as having humidity-controlling salt deposited in the room. However, the warm discomfort can only be dealt with by bringing a vector of cooling such as air conditioner. In addition, according to the analysis of the Givoni diagram, models M1 and M9 have the same hygrothermal index value of 1.9, which reflects a relative proximity of discomfort hours to the comfort zone compared to other model with higher index, *i.e.* 2.0 for concrete.

Figure 7 shows the differences between the temperatures of the indoor environment for the models M1 and M9 from the 1st to the 3rd day of the month of April (the first 72 hours of the hottest month in Ouagadougou). The results show that the average indoor temperature for the model M9 is lower than that of the model M1 in most of the time (51% of the time calculated on the base of the data plotted on Figure 7). From this difference ("Delta M9-M1"), it can be inferred that the model M9 gets hotter slower than model M1 during the heating phases, but it reaches higher temperature. The same analysis can be made on the cooling phases, but this time, the model M9 is more suitable. These imply that the masonry in model M9 (CEB with 20% CCR) absorbs and releases the heat slower than that in model M1 (hollow cement blocks). It is important to note that the cooling phases are longer than the heating phases. Furthermore, from the heat capacities given in Table 3 and Table 5, it can be inferred that CEB stabilized with CCR have higher heat capacities than cement blocks (938 $J \cdot kg^{-1} \cdot K^{-1}$ for 20% CCR-CEB and 600 $J \cdot kg^{-1} \cdot K^{-1}$ for hollow cement blocks). This implies that CEB can stock 56% more heat than cement blocks.

Figure 8 further shows that the depth of the penetration of heat flux of the

model M9 (9.2 cm) is lower than that of the model M1 (14 cm). The depth of penetration indicates, on a time period of 24 hours, how deep the heat flux would penetrate into the wall. This implies that the flux of heat takes more time to get through the CEB than the cement blocks. This further explains the lag observed on the peak temperature due to the slow process of heating/cooling of the CEB (**Figure 7**). It additionally explains the fact that even if the 20% CCR-CEB has a better thermal behavior than the cement blocks, the model M9 reach higher indoor temperatures when the outdoor temperature is at its highest level. With lower external temperatures, this behavior of the CEB becomes favorable for the building, the CEB stores more coolness and deliver it on a longer time.

On these bases, different formulas of CEB stabilized with CCR are more suitable for maintaining the temperature set in the building much longer than the conventional materials such as cement blocks and concrete, and thus would economize the energy consumption if any cooling systems were used. Moreover, the results suggest that stabilization of CEB with CCR not only improved their mechanical performances [18] but also their thermal behavior compared to non-stabilized CEB. Indeed, the previous study [18] reported the positive effects of stabilizing a clayey soil with the same CCR on the mechanical performances of CEB. The results from the present study show the improvement of the thermo-optical properties of CEB.

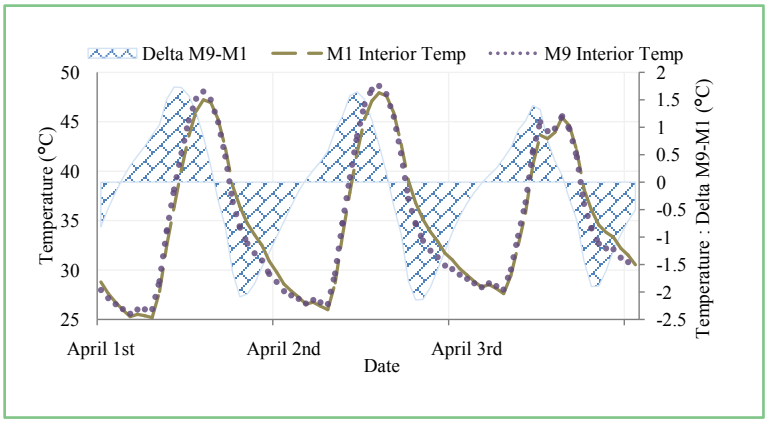

Figure 7. Differences between models M1 and M9 on indoor temperatures.

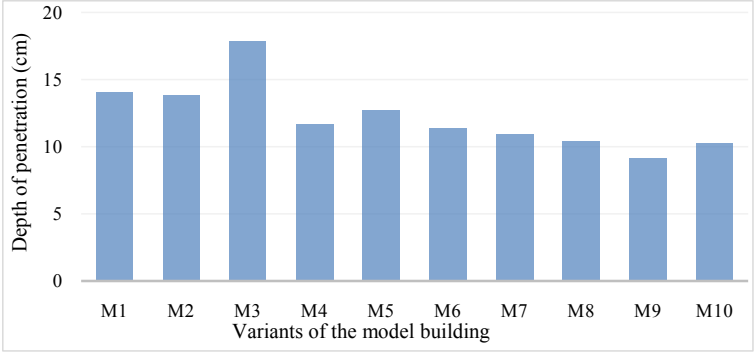

Figure 8. Depth of the penetration of heat flux for different models.

3.3. Evaluation of the Cost

Figure 9 shows the cost of the energy consumed in a year if the air conditioning system (ACS) were used to maintain the indoor temperature not higher than 28˚C during the presence of the occupants. It shows that the model M3 (concrete wall model) represent the highest cost of energy consumed through the year (6830 USD). The reference model M1 comes second in term of cost of energy consumption (6156 USD) while model M9 (CEB with 20% CCR) induces the lowest cost (5566 USD) on energy consumption. This further confirms that the use of CEB stabilized with CCR improves thermal behavior of the buildings, and the higher the CCR content, the better the CEB behaves.

Figure 10 shows the economy made with each model with respect to the model M1. The economy of up to 9.6% that equals to 535 USD (310,000 CFA francs) can be achieved if the building in model M9 (20% CCR-CEB) is air conditioned instead of model M1 (hollow cement blocks). This economy subsequently shows the advantage of using CEB stabilized with CCR instead of the conventional hollow cement blocks. Furthermore, on the environmental point of view, CEB are much more ecological than cement blocks and concrete. By using a by-product as stabilizer, CCR-stabilized CEB would basically become more ecological than those stabilized with cement.

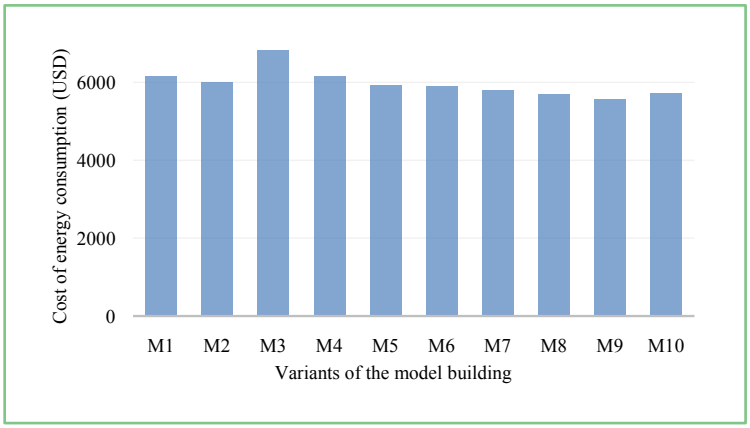

Figure 9. Cost of the energy consumed on cooling by the air conditioning system per year.

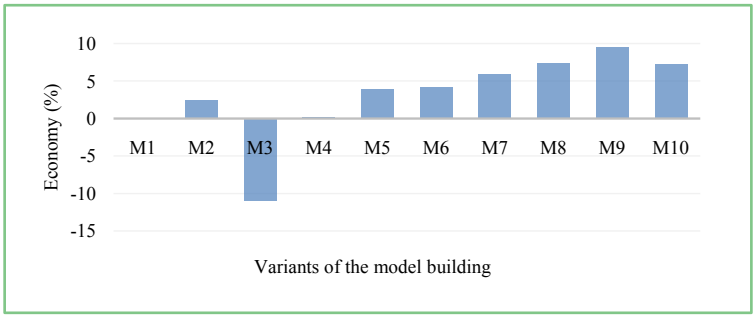

Figure 10. Percentage of money saved on the energy consumption on cooling per year with respect to M1.

4. Conclusions

In this study, different physical and thermal properties were determined on CEB stabilized with an industrial by-product (CCR) for simulating their impact on the thermal comfort in building. The thermal behavior of 10 variants of a 4-room apartment model building was evaluated using the EnergyPlus software. The results showed that stabilization of CEB with CCR impacts their physico-thermal properties and thus the thermal comfort in the model building. More specifically, the following conclusions can be drawn:

- Increasing the content of CCR decreased the apparent density of CEB in the range of 2100 $g \cdot cm^{-3}$ for non-stabilized CEB to 1600 $g \cdot cm^{-3}$ for the 25% CCR stabilized CEB.
- The thermal conductivity and depth of penetration of the heat flux decreased from 1 $W \cdot m^{-1} \cdot K^{-1}$ and 12.7 cm for non-stabilized CEB to 0.5 $W \cdot m^{-1} \cdot K^{-1}$ and 10.2 cm for 25% CCR-stabilized CEB, respectively. The estimated emissivity also decreased from 0.82 for non-stabilized CEB to 0.64 for the 25% CCR-stabilized. These values remain lower than those for the cementitious materials, implying their structural and thermal advantages in terms of reduction of mechanical load and thermal discomfort in buildings.
- The warm discomfort induced by the CEB stabilized with 20% CCR was about 400 hours less than that of the hollow cement blocks. The indoor temperature has also been impacted by the use of CCR-stabilized CEB which favorably get them closer to 28˚C.
- The CCR-stabilized CEB revealed their advantages in terms of energy consumption compared to cementitious materials. They induced economy of up to 9.6% (310,000 CFA francs per year) on energy consumption for cooling in comparison with hollow cement blocks, highlighting their operational benefits.

Nevertheless, it is necessary to assess the durability and hygrometric properties of CCR-stabilized CEB, as well as the investment cost, for drawing definitive conclusions on their economic and environmental impacts.

Acknowledgements

This work was supported by the "Académie de la Recherche et de l'Enseignement Supérieur" of the "Fédération Wallonie-Bruxelles (Belgium)-Commission de la Coopération au Développement (ARES-CCD) as part of an international research and development project "Improving the quality of earth-based housing in Burkina Faso, PRD2016-2021". Burkina Industrial Gas (BIG) company provided the calcium carbide residue used in the present study free of charge.

Conflicts of Interest

The authors declare no conflicts of interest regarding the publication of this paper.

References

[1] Magnier, L. and Haghighat, F. (2010) Multiobjective Optimization of Building Design Using TRNSYS Simulations, Genetic Algorithm, and Artificial Neural Network. *Building and Environment*, **45**, 739-746. https://doi.org/10.1016/j.buildenv.2009.08.016

[2] Eisenhower, B., O'Neill, Z., Narayanan, S., Fonoberov, V.A. and Mezić, I. (2012) A Methodology for Meta-Model Based Optimization in Building Energy Models. *Energy and Buildings*, **47**, 292-301. https://doi.org/10.1016/j.enbuild.2011.12.001

[3] MUH (2017) Annuaire Statistique 2016. Ministère de l'Urbanisme et de l'Habitat, Burkina Faso, Ouagadougou.

[4] Traoré, A. (2003) La problématique des matériaux locaux de construction dans le développement du logement a Ouagadougou. Mémoire de Maitrise (Option Géographie Urbaine). Université de Ouagadougou, Ouagadougou.

[5] Abdullah, A.H., Razman, R., Noh, M.S. and Ibn Abd Wahid, A.Z. (2010) Thermal and Structural Properties of Compressed Earth Brick (Laterite Soil). *Proceedings of the International Postgraduate Conference on Engineering*, Perlis, 16-17 October 2010.

[6] Doubi, H.G., Kouamé, A.N., Konan, L.K., Tognonvi, M. and Oyetola, S. (2017) Thermal Conductivity of Compressed Earth Bricks Strengthening by Shea Butter Wastes with Cement. *Materials Sciences and Applications*, **8**, 848-858. https://doi.org/10.4236/msa.2017.812062

[7] Tatane, M., Akhzouz, H., Elminor, H. and Feddaoui, M.M. (2018) Thermal, Mechanical and Physical Behavior of Compressed Earth Blocks Loads by Natural Wastes. *International Journal of Civil Engineering and Technology*, **9**, 1353-1368.

[8] Zakham, N., *et al.* (2018) Influence of Cement Content on the Thermal Properties of Compressed Earth Blocks (CEB) in the Dry State. *MATEC Web of Conferences*, **149**, Article ID: 01059. https://doi.org/10.1051/matecconf/201814901059

[9] Miralles, J.A.L., Orzáez, M.J.H. and García, C.M. (2018) Comparative Study into the Environmental Impact of Traditional Clay Bricks and Mixed with a Biological Ingredient Using Life Cycle Analysis. *Sustainability*, **10**, 2917. https://doi.org/10.3390/su10082917

[10] Petkar, S.S. (2014) Environmental Impact of Construction Materials and Practices. PhD Thesis, National Institute of Construction Management and Research, Pune.

[11] Üçer, D. (2012) Life Cycle Assessment of Masonry Wall Types Using Simulation Technique. Doctoral Dissertation, Master Thesis, Middle East Technical University, Ankara.

[12] Bueno, C., Rossignolo, J.A. and Ometto, A.R. (2012) Comparative Life Cycle Assessment: Structural Masonry of Concrete and Clay Blocks. *International Symposium on Life Cycle Assessment and Construction*: *Civil Engineering and Buildings*, Nantes, 10-12 July 2012, 223-230.

[13] CDI (1998) Compressed Earth Blocks: Standards Guide-Technology Series No. 11, CRA-Terre-EAG. Brussels-Belgium.

[14] ASHRAE (2004) ASHRAE Standard 55: Thermal Environmental Conditions for Human Occupancy. ANSI/ASHRAE, American Society of Heating, Refrigerating and Air-Conditioning Engineers, Atlanta.

[15] Elenga, R.G., Mabiala, B., Ahouet, L., Goma-Maniongui, J. and Francois, G. (2011) Characterization of Clayey Soils from Congo and Physical Properties of Their Compressed Earth Blocks Reinforced with Post-Consumer Plastic Wastes. *Geoma-*

terials, **1**, 88-94. https://doi.org/10.4236/gm.2011.13013

[16] Villamizar, M.C.N., Araque, V.S., Reyes, C.A.R. and Silva, R.S. (2012) Effect of the Addition of Coal-Ash and Cassava Peels on the Engineering Properties of Compressed Earth Blocks. *Construction and Building Materials*, **36**, 276-286. https://doi.org/10.1016/j.conbuildmat.2012.04.056

[17] Taallah, B. and Guettala, A. (2016) The Mechanical and Physical Properties of Compressed Earth Block Stabilized with Lime and Filled with Untreated and Alkali-Treated Date Palm Fibers. *Construction and Building Materials*, **104**, 52-62. https://doi.org/10.1016/j.conbuildmat.2015.12.007

[18] Nshimiyimana, P., Miraucourt, D., Messan, A. and Courard, L. (2018) Calcium Carbide Residue and Rice Husk Ash for Improving the Compressive Strength of Compressed Earth Blocks. *MRS Advance*, **3**, 2009-2014. https://doi.org/10.1557/adv.2018.147

[19] Nshimiyimana, P., Messan, A., Zhao, Z. and Courard, L. (2019) Chemico-Microstructural Changes in Earthen Building Materials Containing Calcium Carbide Residue and Rice Husk Ash. *Construction and Building Materials*, **216**, 622-631. https://doi.org/10.1016/j.conbuildmat.2019.05.037

[20] Horpibulsuk, S., Phetchuay, C. and Chinkulkijniwat, A. (2013) Strength Development in Silty Clay Stabilized with Calcium Carbide Residue and Fly Ash. *Soils and Foundations*, **53**, 477-486. https://doi.org/10.1016/j.sandf.2013.06.001

[21] AFNOR (2010) Concrete-Testing Hardened Concrete-Testing Porosity and Density. NF P18-459. Saint-Denis.

[22] Ndiaye, K. (2016) Etude numérique et expérimentale du stockage d'énergie par les matériaux cimentaires. Doctorat de l'Université de Toulouse, Université Toulouse III Paul Sabatier.

[23] Marti, K. (2002) Catalogue d'éléments de construction avec calcul de la valeur U Cons-truction neuve. Office fédéral de l'énergie OFEN, Schüpfen.

[24] Gaffey, M.J. (1978) Optical and Spectral Proprieties of the Low Albedo Meteorites: Applications to the Interpretation of the Spectra of Dark Asteroids. *Lunar and Planetary Science*, **9**, 362-364.

[25] Henninger, J.H. (1984) Solar Absorptance and Thermal Emittance of Some Common Spacecraft Thermal-Control Coating. NASA Sci. Tech. Inf. Branch, Washington DC.

[26] ASHRAE (2011) ASHRAE Handbook. HVAC Applications, SI Edition American Society of Heating, Refrigerating and Air Conditioning Engineers, Atlanta.

[27] Clarke, J.A., Yaneske, P.P. and Pinney, A.A. (1990) The Harmonisation of Thermal Properties of Building Materials. BRE.

[28] ASHRAE (2010) ASHRAE STANDARD Standard Method of Test for the Evaluation of Building Energy Analysis Computer Programs, ANSI/ASHRAE Addendum. ANSI/ASHRAE Standard 140-2007. Atlanta.

[29] EnergyPlus (2012) Introduction to EnergyPlus. GARD Analytics.

[30] Akbari, P., Levinson, H., Berdahl, R., Akbari, H., Levinson, R. and Berdahl, P. (1996) ASTM Standards for Measuring Solar Reflectance and Infrared Emittance of Construction Materials and Comparing Their Steady-State Surface Temperatures. University of North Texas Libraries, Denton. https://digital.library.unt.edu/ark:/67531/metadc680781

[31] Coulibaly, Y., Thiombiano, G. and Traoré, Y.M. (1998) Climat et confort thermique. *Sud-Sciences et Technologies*, **2**, 22-27.

[32] Visitsak, S. and Haberl, J.S. (2016) An Analysis of Design Strategies for Climate-Controlled Residences in Selected Climates. *IBPSA-USA National Conference*, Boulder, 4-6 August 2004, 1-11.

[33] Île-de-France, A. and ICEB (2014) Confort d'été passif. ISBN EAN.

[34] Lucas, F., Adelard, L., Miranville, F., Garde, F. and Boyer, H. (2006) Utilisation d'outils de simulations dynamiques pour l'optimisation des performances d'un bâtiment en climat tropical. ESIM, 233-240.

[35] Longo, T.A., Melo, A.P. and Ghisi, E. (2011) Thermal Comfort Analysis of a Naturally Ventilated Building. 12*th Conference of International Building Performance Simulation Association*, Sydney, 2004-2010.

[36] Manioğlu, G. and Yılmaz, Z. (2006) Economic Evaluation of the Building Envelope and Operation Period of Heating System in Terms of Thermal Comfort. *Energy and Buildings*, **38**, 266-272. https://doi.org/10.1016/j.enbuild.2005.06.009

[37] Givoni, B. (1992) Comfort, Climate Analysis and Building Design Guidelines. *Energy and Buildings*, **18**, 11-23. https://doi.org/10.1016/0378-7788(92)90047-K

[38] Toftum, J. (1998) Upper Limits of Air Humidity for Preventing Warm Respiratory Discomfort. *Energy and Buildings*, **28**, 15-23. https://doi.org/10.1016/S0378-7788(97)00018-2

[39] Sonabel (2008) Grille Tariffaire. Société Nationale d'Electricité, Ouagadougou.

[40] Arnold, J., Janssens, D. P. M, A., De Paepe, M. and D. P. M, (2005) Effect of Moisture Inertia Models on the Predicted Indoor Humidity in a Room. 26*th AIVC Conference*, Brussels, 21-23 September 2005, 287-294.

[41] Ramos, N.M. and de Freitas, V.P. (2012) The Evaluation of Hygroscopic Inertia and Its Importance to the Hygrothermal Performance of Buildings. In: Delgado, J., Ed., *Heat and Mass Transfer in Porous Media*, Advanced Structured Materials, Vol. 13, Springer, Berlin, Heidelberg, 25-45. https://doi.org/10.1007/978-3-642-21966-5_2

[42] Bairi, A., Gomez-Arriaran, I., Sellens, I., Odriozola-Maritorena, M. and Perez-Iribarren, E. (2017) Hygroscopic Inertia Influence on Indoor Environments: Moisture Buffering. *Proceedings of the* 13*th International Conference on Heat Transfer*, *Fluid Mechanics and Thermodynamics*, Portoroz, 17-19 July 2017, 538-541.

Definition of Terms

ACS	Air conditioning system
ASHRAE	American society of heating, refrigerating and air-conditioning Engineers
BSSR	Back side solar reflectance at normal incidence
BSVR	Back side visible reflectance at normal incidence
CCR	Calcium carbide residue
CEB	Compressed earth block
Cp	Specific heat
e	Width (thickness)
FSSR	Front side solar reflectance at normal incidence
FSVR	Front side visible reflectance at normal incidence
g	Solar transmittance at normal incidence
HI	Hygrothermal index
OWC	Optimum water content
Uf	Thermal transmittance value on the windows' frames
αs	Solar absorptivity value (solar absorptance)
αth	Thermal absorptivity value (emissivity of the material)
αv	Visible absorptivity value (visible absorptance)
ε	Front and back side infrared hemispherical emissivity
λ	Thermal conductivity
ρ	Density
τl	Visible transmittance at normal incidence